
Effects of the topology and delayed connections in the synchronization properties of a neuronal network

Memoria de investigación presentada por Guadalupe C. García, en el Departamento de Física de la UIB, el 13 de Septiembre de 2010.

Esta memoria de investigación ha sido dirigida por el Dr. *Claudio Mirasso Santos*, profesor del Departamento de Física de la UIB, y el Dr. *Víctor M. Eguíluz* asociado al Instituto de Física Interdisciplinar y Sistemas Complejos (UIB-CSIC).

Contents

Preface	1
1. Introduction	3
1.1. Electrophysiology of Neurons	3
1.1.1. Nernst Potential	5
1.1.2. Ionic Currents	6
1.1.3. Voltage-Dependent Conductances	7
1.2. Neuron Models	10
1.2.1. The Hodgkin-Huxley Model	10
1.3. Intercellular Communications	13
1.3.1. Chemical Synapses	13
1.3.2. Gap Junctions	15
1.4. Synchronization	15
1.4.1. Phase of Oscillation	15
1.4.2. Synchronization Indexes	16
1.4.3. Phase Response Curve	17
1.5. Networks	19
1.5.1. General Properties	19
1.5.2. The Small world property	20
1.5.3. Scale-free distributions	20
2. Single neurons as elemental constituents of networks	21
2.1. Effects of the temporal dynamics of synaptic activation on the PRC	22
2.2. Conduction delays in the connections	23
3. Neural Networks	27
3.1. Effects of the topology	27
3.1.1. Homogeneous delay	27
3.1.2. Heterogeneous delays	30
3.1.3. Heterogeneous currents	33
4. Conclusions	35
Bibliography	39

Curriculum Vitae

I

Preface

A prominent feature of many complex system is their ability to self-organize. One characteristic example of such behavior is the phenomenon of synchronization. Synchronization refers to the emergence of a precise timing between the constituent elements as a result of mutual interaction [1]. This coherent activity arises in a variety of systems such as mechanical oscillators, lasers, chemical reactions, cell populations, and social behaviors. In particular, neuronal synchronization is a fundamental mechanism for the establishment of temporal coordination in the brain. A large number of experiments associates temporal correlations with cognitive and behavioral brain functions [2]. Moreover, converging evidence from different studies suggest that abnormal and abrupt synchronized activity of neurons might play a key role in brain diseases as schizophrenia [3] or epilepsy.

Generally the behavior of complex systems is sculpted by multiple and weak interactions with similar agents. This is the case of nerve cells whose communication and coordination rely on the network in which they are embedded. In this work we study how the network structure and axonal conduction delays alter the temporal coordination of coupled neurons. We find: i) at a local scale, that interacting neurons display in-, out- and anti-phase firing, ii) at a global scale, random connections are required for a coordinated firing, iii) axonal latencies give rise to a resonant effect with the internal period of the oscillatory neurons.

To gain insight into the effects of the delay in the synchronization properties, we will consider two kind of delay configurations: one in which the delays are homogeneous and another in which they are heterogeneous. Since experimental data about axonal distributions of conduction velocities in fibers is limited, specially in the case of humans, we explore different distribution shapes modeled as a general gamma distribution function. For heterogeneous delays we observe that global synchronization in a random network is lost when the variance of the delay distribution is large ($\sigma^2 \sim 2 \text{ ms}^2$). On the contrary, the scale free topology is more robust and maintain globally synchronized regions even for larger variances. In this context, we also investigate how the balance between the network synchronizing effect and the dispersive drift caused by inhomogeneities in natural firing frequencies across neurons is resolved.

In the first part of this work we introduce the dynamical system to be studied and some tools that we use in the next chapters, as synchronization

indicators. In Chapter 2, we study single cells properties that can be related to the synchronization phenomena. This is followed by Chapter 3, where we present the main results, to show how the network structure and the dynamics interact to build a macroscopic behavior. Finally, we summarize the results in Chapter 4.

Chapter 1

Introduction

The histological studies of Ramon y Cajal and many others in the 19th century led to the general consensus that the cells of the central nervous system can be divided into two categories: *nerve cells* (or neurons), and *glial cells*.

Despite the fact that the human brain contains an enormous number of nerve cells, which can be classified by its morphological and physiological features into at least thousand different types, all of them share the same basic architecture. They are specialized for generating electrical signals in response to chemical and other inputs, and transmitting them to other cells [4].

Glial cells, in contrast, are not capable of electrical signaling; nevertheless, they have several essential functions in the brain: they support cells, produce the myelin used to insulate nerve axons, guide migration of neurons, regulate properties of presynaptic terminals, etc. [4]. However recent research is changing dramatically the role of glial cells in the brain [5].

In this chapter we first introduce the basic physiological and morphological properties of the neuron, describing its principal properties, including the ion channels and the generation of electrical impulses. This is followed by Section 1.2 devoted to describe the Hodgkin and Huxley neural model. Then, in Section 1.3, we continue with a brief description of the chemical and electrical process, by which the information encoded by action potentials is passed on at synaptic contacts to the next cell, a process called *synaptic transmission*. In Section 1.4 we briefly overview the phenomenon of synchronization in dynamical systems and define some useful tools to characterize synchronization. Finally, in Section 1.5 we review some fundamental properties of complex networks.

1.1. Electrophysiology of Neurons

Neurons are the basic structural components of the brain. A neuron is an individual cell, specialized by architectural features that enable fast changes of voltage across its membrane as well as voltage changes in neighboring neurons. Four morphological regions can be distinguished in a neuron: the cell

body or soma, the dendritic branches, the axon, and presynaptic terminals. Each region plays a different role in the generation, propagation and transmission of signals between nerve cells [4].

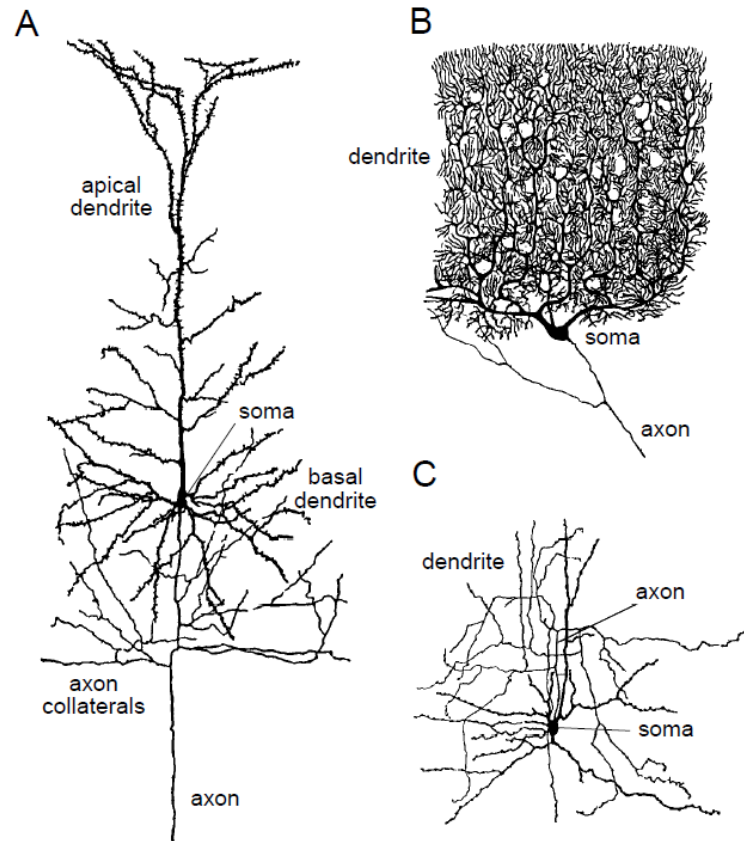


Figure 1.1: Diagrams of three schematic neurons, adapted from [6]: A) a cortical pyramidal cell. B) a Purkinje cell. C) a Stellate cell of the cerebral cortex.

The nucleus of the cell is contained in the soma, the metabolic center. From there the extensive branching arises, the most characteristic specialization for communication that they have. The dendrites are the principal receptors for collecting and integrating incoming signals from other nerve cells. Moreover, a variety of branching shapes can be observed in different areas of the brain (see Figure 1.1); the number of inputs that a neuron receives depends on the complexity of the dendritic tree. In contrast, the axon extends away from the soma, and its principal role is to carry information away from the cell body and towards the output terminal. It can conduct signals, called *action potentials*, along distances ranging from 0.1 mm to 3 m. The nerve impulses, with amplitude of 100 mV and duration of about 1 ms, are initiated at the origin of the axon and from there they are conducted down the axon [6]. Axons terminate at the synapses where the voltage signal opens ion channels

that mediate the release of neurotransmitters into the synaptic cleft, a process termed *exocytosis*. The transmitted neurotransmitters diffuse across the synaptic cleft and bind to the receptors on the postsynaptic cell membrane. This process opens or closes ion channels altering the membrane potential of the postsynaptic neuron (see Section 1.3 for a detailed description of the chemical synapses).

1.1.1. Nernst Potential

Neuronal signaling depends on rapid changes in the membrane potential of nerve cells; this electrical activity is sustained and propagated via ionic currents through neuron membranes. A wide variety of membrane ion channels allow ions, predominantly sodium (Na^+), potassium (K^+), calcium (Ca^{+2}), and chloride (Cl^-), to move into and out of the cell. The flow of ions across the membrane is controlled by channels that open and close in response to voltage changes, and both internal and external signals [7].

As in all cells, neurons are enclosed by a membrane, which acts as a boundary separating the interior of the cell from the external environment. Its selectively permits the passage of some material and restricts the passage of others. This insulating feature causes the membrane to act as a capacitor separating the charges from the interior to the exterior surface. To maintain ion differences concentration across the membrane, there are selective pumps that expend energy to carry ions against their concentration gradient. A potential difference across the cell is created by the difference ion concentration in both sides of the membrane. These two forces, the concentration and electric potential gradients, regulate the flow of ions through the membrane, governing the dynamics of the cell [8].

The Nernst Equation describes how a difference of ionic concentrations between two phases can result in a potential difference across them [8]. As an example, in the interior of the cell the concentration of K^+ ions is higher than outside, these ions diffuse out of the cell because of the gradient, producing an outward current. The positive charge accumulates in the exterior of the cell, creating an electrical potential across the membrane. The diffusion process is slowed down by the electrical potential, since the K^+ ions are repelled from the positive charge from the exterior of the membrane and attracted to the negative charge into the interior. At some point the concentration gradient and the electrical potential gradient counterbalance these opposite forces and the net current is zero. The value of such equilibrium potential is given by the Nernst equation [7]:

$$E_{\text{ion}} = \frac{RT}{zF} \ln \frac{[\text{Ion}_{\text{out}}]}{[\text{Ion}_{\text{in}}]}, \quad (1.1)$$

where T is the temperature in Kelvin degrees, F is the Faraday's constant (96,480 coulombs/Mol), R is the universal gas constant (8,315 mJ/(K Mol)), z is

the valence of the ion, $[\text{Ion}_{\text{out}}]$ and $[\text{Ion}_{\text{in}}]$ are the ions concentration outside and inside the cell. Equilibrium potentials for K^+ ions, called reversal potential, E_k , typically fall in the range between -70 mV to -90 mV, for Na^+ ions the equilibrium potentials E_{Na} , is 50 mV or higher and E_{Ca} for Ca^{+2} channels is higher, around 150 mV [6].

1.1.2. Ionic Currents

The potential of the extracellular fluid outside a neuron is defined, by convention, to be zero. In an inactive state a neuron has an excess of internal negative charge that causes the potential to be negative. At this equilibrium point the currents of ions are balanced, but if the balance of ion flow is modified by opening or closing channels the potential can change [6]. We label the different types of channels in a cell membrane with an index x , where x can be K, Na, Cl, Ca, etc. The net current of the x ion is proportional to the difference of the membrane potential (V) and the reversal potential of the specific ion (E_x), $(V - E_x)$, the electrochemical driving force. The membrane current per unit area is written then as:

$$I_x = g_x(V - E_x), \quad (1.2)$$

where the positive parameter g_x (mS/cm²) is the x conductance per unit area due to these channels. We assume that the reversal potential (E_x) of the specific ion x remains constant, this means that the restorative mechanism, the ionic pumps, acts on a time scale that does not allow the battery to run down [9]. The total membrane current (I_m) over the different types of channels is:

$$I_m = \sum_x g_x(V - E_x). \quad (1.3)$$

Generally, ionic currents in neurons are not Ohmic, the conductance depends not only on time but also on membrane potential, pharmacological agents, neurotransmitters, etc [7]. The variety, complexity and diversity of neuronal dynamics are in part due to this variability [6].

It is possible to represent the electrical properties of the cell in terms of an equivalent circuit as the one shows in Figure 1.2. If we assume that the membrane acts as a capacitor, separating charge from the interior to the exterior, the capacitive current I_c can be written as follow:

$$I_c = C \frac{dV}{dt}, \quad (1.4)$$

where C is the capacitance of the membrane and V is the membrane potential (the difference between the inside and outside). Applying the Kirchoff's law to the circuit of the Figure 1.2 we get that the total current I is:

$$I = \sum_x I_x + I_c, \quad (1.5)$$

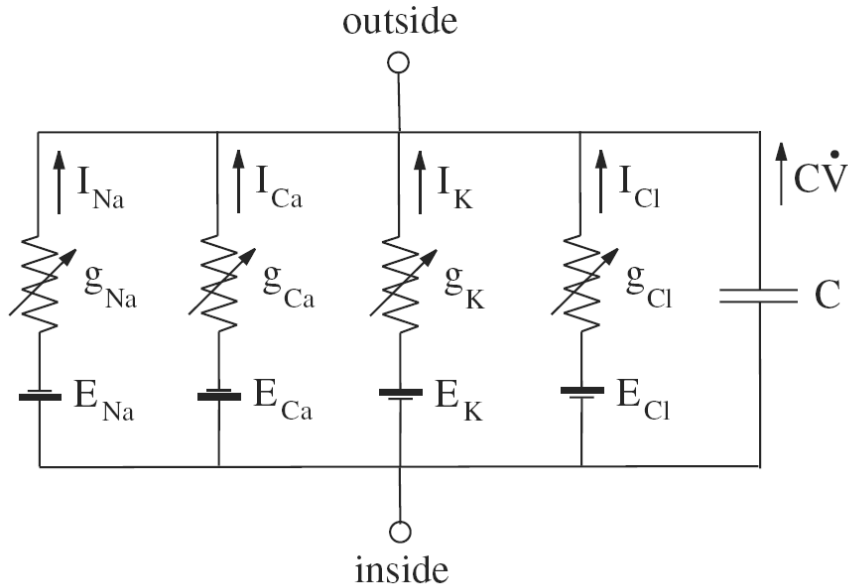


Figure 1.2: Equivalent circuit diagram for one-compartment neuron model (Adapted from Izhikevich 2007 [7]).

where I_c is the capacitive current and I_x the ionic current. This equation can be written as:

$$C \frac{dV}{dt} = - \sum_x I_x + I. \quad (1.6)$$

If there are not additional currents then $I = 0$, but usually a neuron is not isolated and receives synaptic currents or external applied currents. These types of models described by a single variable V are known as single compartment models.

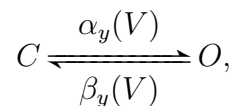
1.1.3. Voltage-Dependent Conductances

Among the cells of the body, only neurons (and muscle cells) can generate electrical pulses that can carry out rapidly over long distances [4]. In the last sections we saw how the membrane potential can change by the influx of ions across the cell membrane. In this section we will see how the electrical pulses are generated due to the nonlinearities of the active membrane conductances. The fundamental excitable elements of nerve cells are ion channels. They can be thought to have gates that modify the permeability of the pore to ions. The gates can be divided into two types: those that open channels (activation) and those that close channels (inactivation). These gates are controlled by the membrane potential, intracellular and extracellular agents (as neurotransmitters).

In 1938 Kenneth Cole and Howard Curtis made an experiment that gave a clue about how are generated actions potentials in the squid giant axon [10]; they measured ionic conductances during the generation of an action potential and observed a dramatic increase in their values. Later on, the voltage clamp experiments done by Hodgkin and Huxley confirmed these observations, and systematically varying the membrane potential they measured the conductances of sodium and potassium, giving a complete description of the ionic mechanism of spikes' generation [11]. They observed that a brief depolarization can activate voltage-dependant sodium conductances, generating a positive feedback loop; the membrane potential increases, the sodium channels open generating an inward sodium current that tends to increase even more the membrane potential. Something similar occurs with the potassium channels, the channels open and the K^+ ions flows outward. Nevertheless, they differ in two aspects: (1) their rate of onset and offset and (2) their inactivation. The sodium conductances turn on and off more rapidly than the potassium, at all potentials. Moreover, the sodium conductances have inactive gates that turn off the channels where the others do not; the potassium current is flowing until the membrane is repolarized.

The generation of an action potential involves a series of steps: when a perturbation depolarizes the membrane, as we said, the Na^+ channels open rapidly and depolarize further the membrane, generating a quick excursion of the potential to values close to 100 mV. The duration of the spike is limited by two factors: the slower outward currents of K^+ , that are also activated when the membrane is depolarized and the gates of Na^+ channels that become inactive. A transient hyperpolarization (brief increase in the negativity) follows the action potential in almost all neurons, because the K^+ channels are slow and do not have inactive gates [12].

The transition between open and close states in a single channel is stochastic by nature. The probability to find the activation gate in the open state is denoted with the letter m for Na^+ and n for K^+ ions, and the probability to find the inactivation gate in the open state is denoted by h for Na^+ ions. In the Figure 1.3 we plot a schematic diagram of the gating membrane channels. The simple cartoon of gating is a channel switching between two states, one with the pore open and other with the pore close. This kinetic model takes the form of the following diagram:



where $C(O)$ corresponds to the close (open) state and the transition probabilities $\alpha_y(V)$ and $\beta_y(V)$ depend on the membrane potential. The fraction of open channels is denoted by y . The rate of change of y has two contributions: the gates close at time t , that change to open at time $t + dt$ with the opening rate $\alpha_y(V)$ and the gates open at time t that become close at $t + dt$, at the close rate

$\beta_y(V)$. The difference between the two fluxes represents the rate of change in y over time:

$$\frac{dy}{dt} = \alpha_y(V)(1 - y) - \beta_y(V)y, \quad (1.7)$$

This equation can be written in other useful form:

$$\tau_y(V) \frac{dy}{dt} = y_\infty(V) - y \quad (1.8)$$

where $\tau_y(V) = \frac{1}{\alpha_y(V) + \beta_y(V)}$ and $y_\infty(V) = \frac{\alpha_y(V)}{\alpha_y(V) + \beta_y(V)}$; $y_\infty(V)$ represents the fraction of open channels at equilibrium at the membrane potential V . Thus, at a fixed V y approaches the limiting value y_∞ exponentially with time constant $\tau_y(V)$.

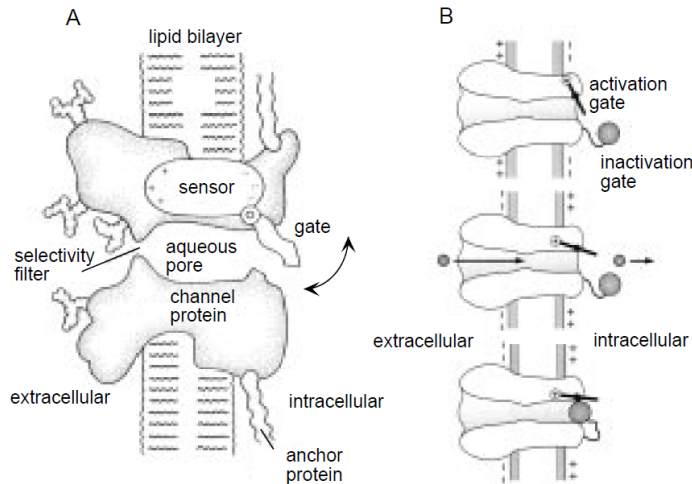


Figure 1.3: A schematic diagram of membrane channels gates. A) a cartoon of a persistent conductance: a gate is open or close according to the membrane potential. The channels are also selective to specific ions. B) In this draw we can observe two types of gates, one of activation and the other of inactivation. Only the middle panel shows an activated channel that allows the passage of ions. Figure adapted from [6].

In the case of Na^+ channels there are two different gates, for activation (m) and inactivation (h), that are independent. So, the probability to find a fraction of Na^+ channels open is proportional to mh . In the last section, we write the membrane current per unit area for a specific ion as a conductance (per unit area) times the potential (equation 1.2). The value of g_y is proportional to the density of ion channels (maximum conductance) multiplied by the probability to find the channels open: $g_y = g_{max}y$.

1.2. Neuron Models

In the following section we describe one of the most important neuron models proposed by Hodgkin and Huxley. Several models derived from this, often called Hodgkin-Huxley type models or conductance-based models, they can describe spike generation in almost all neurons recorded [7]. It is important to mention that we are considering nerve cells as an idealization of point neuron (electrically compact); therefore, we are not considering propagation of the spikes along the axon neither integration of synaptic input over the dendritic tree.

1.2.1. The Hodgkin-Huxley Model

Hodgkin and Huxley wrote, in 1952, a series of five papers describing and modeling their pioneer experimental work on the generation of action potentials in the giant squid axon. They developed one of the most important models of nerve cells in computational neuroscience.

The HH model is a four-dimensional dynamical system, its state is determined by the membrane potential (V), and the gating variables n for persistent K^+ and m and h for transient Na^+ currents [11]. As it was explain in section 1.3, for a small patch of membrane the total current has two contributions: one from the capacitive current and the other from ionic currents. These contributions can be written as in equation (1.6). The complete set of ordinary differential equations for the HH is described below:

$$C_m \dot{V} = I - g_{Na} m^3 h (V - V_{Na}) - g_K n^4 (V - V_K) - g_L (V - V_L), \quad (1.9)$$

$$\dot{n} = (n_\infty(V) - n) / \tau_n(V),$$

$$\dot{m} = (m_\infty(V) - m) / \tau_m(V),$$

$$\dot{h} = (h_\infty(V) - h) / \tau_h(V),$$

where the dependent rates where fitted to:

$$\alpha_n(V) = 0.01 \frac{V + 55}{1 - \exp(-0.1(V + 55))},$$

$$\beta_n(V) = 0.125 \exp(-0.0125(V + 65)),$$

$$\alpha_m(V) = 0.1 \frac{V + 40}{1 - \exp(-0.1(V + 40))},$$

$$\beta_m(V) = 4 \exp(-0.0556(V + 65)),$$

$$\alpha_h(V) = 0.07 \exp(-0.05(V + 65)),$$

$$\beta_h(V) = \frac{1}{1 + \exp(-0.1(V + 35))}, \quad (1.10)$$

As we can see in the equation 1.9, three major currents control the potential: a sodium, a potassium and a leaky current. From their measurements they inferred that the potassium conductance involves four independent activation gates (the term n^4 in the equation 1.9), and the sodium conductance involves three independent activation gates (m^3) and one inactivation gate h . The exponents of m and n were chosen to best fit the experimental data. To illustrate the generation of an action potential with the model in Figure 1.4 we plot the membrane potential, the gating variables and the currents after an injected pulse of current. It is interesting to notice the different time scales in the fast activation of sodium current and the relatively slower negative feedback from potassium current and sodium inactivation, as we mentioned before in Section 1.1.3.

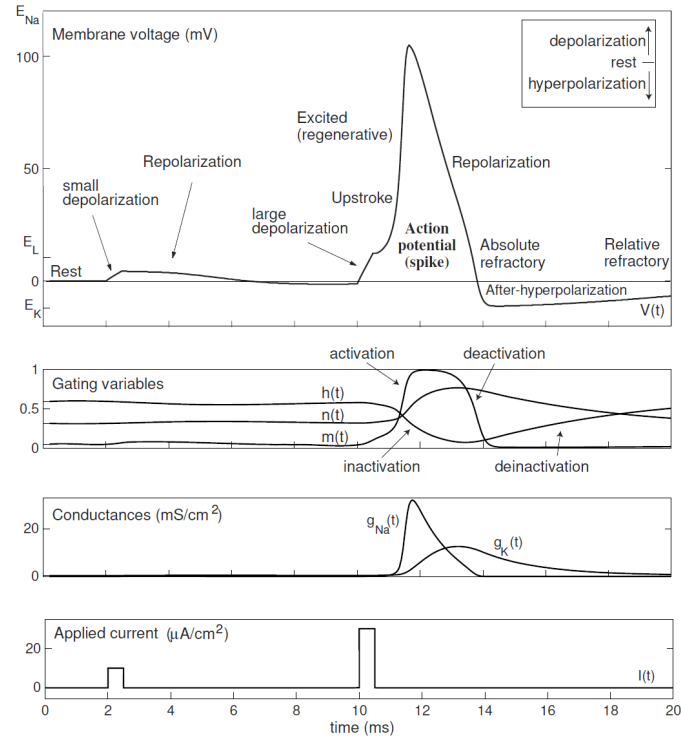


Figure 1.4: Generation of an action potential in the Hodgkin and Huxley model in response to a current pulse. In the top panel we plot the membrane voltage (mV) in response to a small positive perturbation and an intermediate pulse that generates an action potential. In the other panels we plot the gating variables, the conductances and the applied current. Figure adapted from [7]. In this schematic draw the rest membrane potential is shifted to zero as in the original work of Hodgkin and Huxley.

The maximal conductances and reversal potentials are: $g_{Na} = 120 \text{ mScm}^{-2}$, $g_K = 36 \text{ mScm}^{-2}$ and $g_L = 0.3 \text{ mScm}^{-2}$, $E_{Na} = 50 \text{ mV}$, $E_K = -77 \text{ mV}$ and $E_L = -54.5 \text{ mV}$. The values of the reversal potentials and transition rates are taken from [6], which differ from the original values of the HH experiment, because the rest membrane potential is shifted close to zero, for convenience.

1.3. Intercellular Communications

Neurons have the special ability to communicate and interact with other cells. This section is devoted to the cellular mechanism for signaling between neurons. There are primarily two ways for neuron cells to communicate with their neighbors: *electrical* or *chemical*. Electrical synaptic transmissions, also called gap junctions, are rapid and they do not produce inhibitory actions or long changes in the electrical properties of the postsynaptic cell. In contrast, chemical synapses can produce excitatory or inhibitory actions in the postsynaptic cell, and they produce electrical changes that last from milliseconds to minutes. Another major difference is that, in chemical synapses the message is mediated by the release of neurotransmitters from the presynaptic cell and received by receptors in the postsynaptic cell. We will discuss in the following section the main characteristics of both types of synapses. However, we would like to emphasize that synaptic communication in the brain relies mainly on chemical mechanisms [8, 13].

1.3.1. Chemical Synapses

Chemical synaptic transmission begins when an action potential reaches the presynaptic terminal and activates Ca^{+2} channels, generating an influx of Ca^{+2} ions. The rise of intracellular Ca^{+2} concentration causes the vesicles to fuse the presynaptic cell membrane and release the neurotransmitters into the synaptic cleft between pre and postsynaptic sides of the synapse. A neurotransmitter is a chemical substance that will bind to specific receptors in the postsynaptic cell membrane, and initiates changes in its membrane potential [8]. A schematic diagram of this process is represented in Figure 1.5.

Synaptic interactions are traditionally classified as excitatory or inhibitory depending on the effects that produce either depolarizing or hyperpolarizing the membrane potential of the postsynaptic cell. In both cases the activation of the receptors in the postsynaptic cell results in the opening of certain ion channels and, thus, in an excitatory or inhibitory postsynaptic current (called EPSC or IPSC). Glutamate and GABA are the major excitatory and inhibitory neurotransmitters in the brain. In addition, the principal receptors for glutamate are AMPA and NMDA, presenting different characteristics. On the other hand, the principal receptors for GABA neurotransmitters are GABA_A and GABA_B , they also generate ionic currents with different features in the postsynaptic membrane potential [6].

A simplified model of this type of synapses describes the transmitter-activation ion channel as a time dependent conductivity $g_{syn}(t)$. Therefore, when a spike arrives at the presynaptic terminal the channel will open and the conductivity increases. The current through this channel depends also on the postsynaptic membrane potential, as it is detailed below:

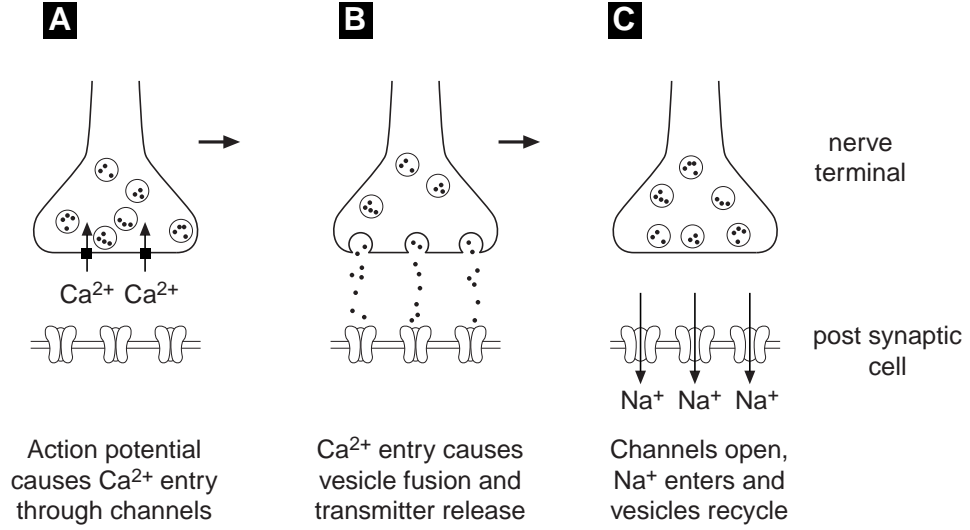


Figure 1.5: Signal transmission in a chemical synapse: A) when a neuron fires, the action potential travels down through the axon and reaches the presynaptic terminal, where the Ca^{+2} channels are activated. B) the rise of the intracellular Ca^{+2} concentration causes the release of neurotransmitters in the synaptic cleft. C) the neurotransmitters bind to specific receptors in the postsynaptic cell and initiate changes in its membrane potential. Figure 6.5 from [9]

$$I_{syn} = g_{syn}(t)(V(t) - E_{syn}), \quad (1.11)$$

where V is the membrane potential of the postsynaptic neuron and E_{syn} is the reversal potential; the specific value of the E_{syn} depends, as before, on the type of channels that are activated (Section 1.1.1). It is common to use a value E_{syn} equal to zero for excitatory synapses and -75 mV for inhibitory synapses [14]. These values of E_{syn} will produce respectively a negative (inward) current and a positive (outward) current; therefore, increasing and decreasing the membrane potential of the cell.

Typically a superposition of exponential functions is used for modeling $g_{syn}(t)$; a standard choice is:

$$g_{syn}(t) = \frac{g_{max}}{\tau_d - \tau_r} (\exp(-t/\tau_d) - \exp(-t/\tau_r)) \quad (1.12)$$

where the characteristic times τ_r and τ_d are the rise and decay time of the synapse. For example, AMPA receptors are characterized by fast response to presynaptic spikes and quickly decaying currents; in contrast NMDA receptors are significantly slower. Moreover, typical values of the rise and decay time for AMPA receptors are ranging between 0.09 ms and 1.5 ms, and between 3 ms and 40 ms for NMDA [14].

To summarize, the net current through the membrane of the postsynaptic neuron is:

$$I_{syn} = - \sum_{spikes} g_{syn} (t - t_{spike}) (V(t) - E_{syn}) , \quad (1.13)$$

where g_{max} is the maximum synaptic conductance, t_{spike} is the time of the presynaptic action potential, and the sum is extended over the train of presynaptic spikes that occur at time t_{spike} .

1.3.2. Gap Junctions

One way that cells can interact is simply by passing ionic currents between each other. This type of synapses is called gap junctions or electrical coupling. Cardiac cells and many others interact by this mechanism, with ions directly flowing from one cell to the other [9]. A major difference between chemical and electrical synapses is that transmission across electrical synapses is extremely rapid, as a consequence of the direct flow of ions from the presynaptic to the postsynaptic cell. Furthermore, gap junctions are bidirectional and localized.

This type of synapse is usually modeled as a net current proportional to the difference between the pre and postsynaptic membrane potential:

$$I_{syn}^i = -g_{syn}(V_j(t) - V_i), \quad (1.14)$$

where I_{syn}^i is the gap-junctional current that flows from cell j to cell i , and g_{syn} is the net coupling conductance of all the junctions.

1.4. Synchronization

In order to study synchronization properties of a neural network in the following chapters, we define in this section some useful tools as the phase of the oscillators, synchronization indexes and phase response curve.

1.4.1. Phase of Oscillation

Regular firing activity of neurons in the brain has been well documented in many areas, for example interneurons in the Hippocampus fire quite regularly [15]. We use this neural oscillators as a motivation to carry our research based on synchronization properties of a network of neural oscillators. To characterize the synchronization in the network we use an order parameter based on the phase difference between elements. We should begin by defining the phase of the oscillators. In general terms, the phase is a mapping of the state of the system along the limit cycle¹ onto the line of real numbers [17].

¹a limit cycle is a periodic solution to a system of differential equations that is stable to small perturbations [16].

Several definitions of the phase are possible and not equivalent. In our case, the phase $\phi_i(t)$ of the spiking neuron i , is defined as a linear interpolation between the time of two pulses [1]:

$$\phi = 2\pi \frac{t - \tau_k}{\tau_{k+1} - \tau_k}, \tau_k \leq t \leq \tau_{k+1} \quad (1.15)$$

where τ_k is the time of the k^{th} spike, and when the neuron is not firing the phase is defined as $\phi_i(t) = 0$. Figure 1.6 illustrates a time trace of the membrane potential of a Hodgkin an Huxley neuron model and the parametrization of its phase.

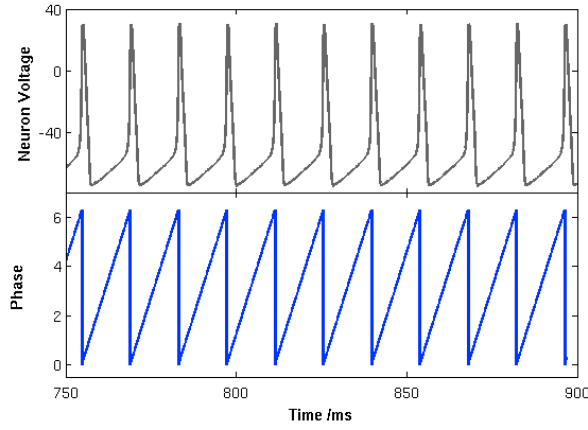


Figure 1.6: Time trace of the membrane potential of one neuron described by the Hodgkin and Huxley model and its phase.

1.4.2. Synchronization Indexes

To characterize the synchronization among neighbors in our network, we employ an indicator $s_i(t)$ defined as follow:

$$s_i(t) = \frac{1}{n_i} \sum_{j \in \nu(i)} \sin^2 \left(\frac{\phi_i(t) - \phi_j(t)}{2} \right), \quad (1.16)$$

where the sum runs over $\nu(i)$ all the neighbors of the neuron i , and n_i is the number of connected neighbors to this neuron. By averaging over elements and integrating in time, we get the local synchronization indicator:

$$S^{loc} = \lim_{T \rightarrow \infty} \frac{1}{T} \int_0^T \left(\frac{1}{N} \sum_{i=1}^N s_i(t) \right) dt, \quad (1.17)$$

This index gives a measure of the local synchronization over the network units.

To characterize the synchronization among all the neurons in the network, we used the index:

$$s'_i(t) = \frac{1}{n_i} \sum_{j=1}^N \sin^2 \left(\frac{\phi_i(t) - \phi_j(t)}{2} \right), \quad (1.18)$$

where the sum now is extended over all the neurons in the network. By averaging over elements and integrating in time, we get the global synchronization indicator:

$$S^{glob} = \lim_{T \rightarrow \infty} \frac{1}{T} \int_0^T \left(\frac{1}{N} \sum_{i=1}^N s'_i(t) \right) dt. \quad (1.19)$$

These two order parameters are zero if the phases of the oscillators are equal, one if they differ by π and 0.5 if they are randomly distributed. To exemplify, I enclose the time traces of two neurons synchronized in-phase and in anti-phase Figure 1.7, with synchronization indexes zero and one respectively.

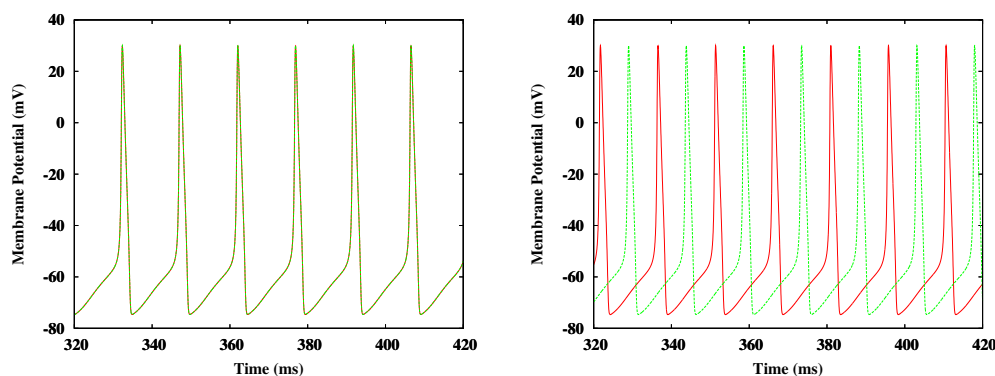


Figure 1.7: Time traces of the membrane potential of two neurons synchronized in-phase (left) and in anti-phase (right), with synchronization indexes zero and one respectively.

1.4.3. Phase Response Curve

As we mention, oscillatory activity is observed in a variety of brain functions [2]. It is possible to characterize the behavior of single units without knowing the precise mechanism of oscillation. The phase response curve provides a powerful tool to characterize this type of activity. If a neuron is in a tonic firing regimen a brief perturbation can change the timing of the following spike. The magnitude of the phase shift of the next spike depends on the

exact timing of the stimulus relative to the phase of oscillation. By stimulating the neuron at different phases, we can measure the phase response curve (also called phase resetting curve PRC, or spike time response curve STRC), defined as [7, 18, 19]:

$$PRC(\phi) = 1 - \frac{T_{new}}{T_0}, \quad (1.20)$$

where T_{new} is the time at which the perturbed spike occurs, T_0 the natural period of oscillation and $\phi = \frac{t_s}{T_0}$ is the time of the stimulus relative to the oscillatory cycle. A positive value of the function means advance of the next spike and a negative value means delay of the next spike. In the case of a Hodgkin and Huxley neuron, the PRC depends not only on the type of synapses but also on the temporal dynamics of synaptic activation. I enclose a PRC of a HH neuron in regular spiking regimen stimulating the cell with a Heaviside step function (equivalent to a small perturbation) and computed with the adjoint method [20] in XPPAUT [21] see Figure 1.8.

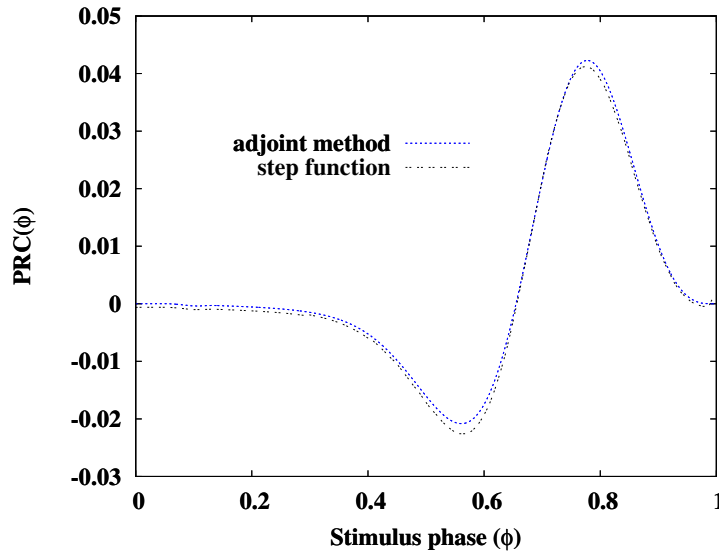


Figure 1.8: Phase response curve of a HH neuron computed with the adjoint method in XPPAUT and stimulated with a Heaviside step function.

We will see in the next section how to relate the shape of the PRC with synchronization properties at least for two identical coupled neurons. PRCs are popular among experimentalist because they provide a way to quantify the behavior of the oscillators. They have been computed for many biological oscillators [18, 19], including neurons [22, 23]. This approach is relevant as

a means of: it is possible to extract main features of neuron models and real neurons that affect the synchronization properties.

1.5. Networks

The behavior of a complex system is shaped by the interactions among their components. Thus, the interaction between the dynamics of the constituent elements and the architecture of the networks is a crucial issue to be studied. During the last two decades a large effort has been devoted to study the evolution, structure and function of complex networks [24, 25, 26], the nodes of the networks can be social agents, molecules, web pages or neurons, for instance. In the next section we introduce some basic definitions and properties of networks that will be used in the next chapters to explore the effect of the network structure into the network dynamics.

1.5.1. General Properties

A complex network can be represented as a graph $G = (N, E)$, its mathematical abstraction. It is composed by a set of N nodes (or vertices), connected by a set of E links (or edges). The degree (or connectivity) k_i of a node i is the number of connections that link it to the rest of the network. The graph G can be represented by a matrix, called adjacency matrix A , with values $a_{ij} = 1$ if a link exists² between node i and j and 0 otherwise. This is a $N \times N$ matrix, where N is the total number of vertices [27].

The simplest topological characterization of a graph is the degree distribution $P(k)$, which indicates the probability of a node chosen at random to have a degree k . The first moment of the distribution $\langle k \rangle$ is the mean degree of G . For example the Erdős-Rényi random graph [28] has a Poisson degree distribution for a large value of N , while the degree distribution of a scale free network is a power law, $P(k) \propto k^{-\gamma}$, where γ is the exponent of the distribution [26].

Graph topology can be described by a variety of measures. In this work we will describe some of them: the average shortest path lengths, diameter and clustering coefficient.

The Path length ($d_{i,j}$) is the minimum number of edges that connect node i with node j , and $L = \langle d_{i,j} \rangle$ is the average shortest path length. Random and complex networks have short mean path lengths while regular lattices have long mean paths [29]. It has an important role in transport and communication within a network. The maximum value of $d_{i,j}$ is called the diameter of the graph.

The clustering coefficient measures the number of connections that exists between the nearest neighbors of a node relative to the maximum number of

²considering undirected graphs

possible connections, average over all vertices. Random networks have low clustering whereas complex networks or regular lattices have high clustering coefficient.

1.5.2. The Small world property

The topology of many real networks, biological, technological or social networks, is neither regular nor random but it lies somewhere in between. On the one hand, there are shortcuts, links that connect distant areas of the network. This means that with a few steps it is possible to link all nodes of the network, having a short characteristic path length. On the other hand, these networks present a high clustering coefficient, like regular lattices, most nodes are connected with a few neighbors vertices. Watts and Strogatz proposed an algorithm to generate this type of network topology [30]. They considered a random rewiring procedure, starting from a regular lattice with N vertices and E links, and they rewire each edge at random with probability p . Therefore, varying the rewiring probability it is possible to construct a regular lattice $p = 0$ (none of the links are rewired) or a random network $p = 1$ where all the edges are rewired. In between $0 < p < 1$ it is possible to find networks with the characteristic described before.

1.5.3. Scale-free distributions

The degree distribution of large networks, as the WWW or citation patterns in science, follows a power law distribution. This means that the probability $P(k)$ that a node interacts with k other nodes decays as $P(k) \propto k^{-\gamma}$ [31]. In biological systems the degree exponent ranges between 2 and 3. These networks present few nodes (or hubs) connected to many others vertices and a large number of poor connected vertices. A power law decay of the degree distribution implies a lack of characteristic scale in the network. Power laws have the property of having the same functional form at all scales. From this feature it comes the term *scale free* networks [25]. Barabási and Albert [31] demonstrated that scale free networks can be originated attaching new vertices by the mechanism of preferential linking.

In Chapter 3 to study the influence of the network structure into the dynamics we implement small world networks, with the algorithm proposed by Watts and Strogatz [30], and scale free networks with the algorithm described by Barabási and Albert [31], both models explained above.

Chapter 2

Single neurons as elemental constituents of networks

Several studies have focused the attention on the synchronization properties of coupled neurons. A major contribution to understand the different process to achieve synchronization among neuron models is based on the analysis of the phase response curve (PRC or phase resetting curve). As we mentioned in the introduction the PRC measures how much a given perturbation can change the time of the next spike in a neural oscillator.

Different types of PRCs have been found. Hansel and collaborators [32] made a distinction between neurons with type I response, with a positive PRC, and neurons with type II, with positive and negative PRC. Neurons with a positive PRC advance the next spike in response to a brief perturbation, while they delay the next spike if the PRC is negative. It has been shown that a pair of coupled neurons with type I PRC can synchronize in-phase with inhibitory synapses, while they can synchronize in anti-phase if the coupling is excitatory. However, fast excitatory connections can produce in-phase synchronization in models with type II PRC and fast inhibitory connections, anti-phase synchronization [33, 34].

It has been also shown that the temporal dynamics of synaptic activation plays a crucial role in determining if excitation or inhibition synchronize spiking responses [33]. As we will see, a way to observe how the timing affects the synchronization is by computing the PRC of a neuron for different rise and decay times of the synapse (see Section 1.3.1). For excitatory synapses and increasing the rise time the negative part of a HH PRC becomes positive, and the neuron loses the capability to delay the next spikes. Therefore, a pair of coupled neurons loses the capability to synchronize in-phase with excitatory synapses.

We begin to explore the PRC of a Hodgkin and Huxley model for different rise time of the synapse. We look how do stable solutions change with these parameters in a network motif of two reciprocally coupled neurons.

We also study the effect of an explicit axonal conduction delay in the con-

nections. It has been shown that the delay can change the stability of different solutions (in-,anti- or out of phase) in coupled neurons modeled by the quadratic integrate and fire [7]. We investigate this effect for two Hodgkin and Huxley neuron reciprocally connected.

2.1. Effects of the temporal dynamics of synaptic activation on the PRC

We begin by computing the Phase Response Curve of an isolated neuron. The neuron receives a constant bias density current of $I = 10 \mu\text{A}/\text{cm}^2$, leading to regular spiking with a period of 14.65 ms. By stimulating the neuron at different phases of the cycle (i.e., time of the stimulus t_s relative to the oscillatory cycle T_0), we can measure the phase response curve (See Section 1.4.3). The PRC can be computed stimulating the neuron with a step function or a delta pulse. We stimulate the neuron with a synaptic current composed by two exponential functions as it was described in Section 1.3.1, mimicking the effect of a chemical synapse. The rise time of the synapse indicates how fast the synaptic current reaches the maximum. If the time rise is small the synapse is fast, while if the rise time is large it takes more time to reach the peak and the synapse is slow. We continue exploring the effect of this parameter on the PRC.

In Figure 2.1 we plot in red the PRC of a neuron with an excitatory fast synapse. The negative part of the curve indicates that the neuron delays the time of the next spike in response to a brief perturbation, and the positive part indicates that the neuron advances the time of the next spike. Therefore, if the stimulus arrives soon after the spike discharge, the neuron delays the next spike. At that time, the neuron is recovering from hyperpolarization. Thus, the potassium current decays and the sodium current de-inactivates (see Figure 1.4), both process are slowed by the depolarization [2], delaying the time of the next spike. If the stimulus arrives in the last part of the cycle, the neuron is ready to fire and it advance the time of the next spike. We will see that, with this type of PRC, a pair of identical coupled neurons can synchronize in-phase (without an explicit axonal delay).

If the rise time of the synapse is larger, the synapse is slow and the shape of the PRC changes. We plot in Figure 2.1 the PRC of a neuron stimulated with a slow synapse, with rise time of 3.5 ms. The neuron loses its ability to delay the time of the next spike, the PRC becomes positive. We observe a transition from type II to type I PRC increasing the rise time of the synapse.

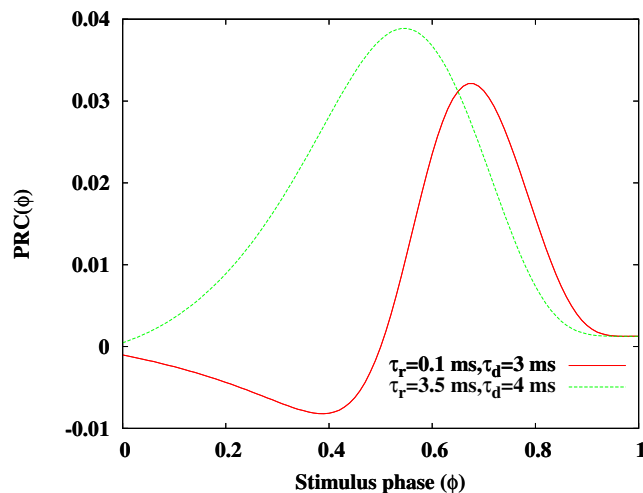


Figure 2.1: Phase Response Curve for a fast (red) and slow (green) excitatory connection, the rise time is 0.1 ms and the decay time is 3 ms for the red curve and the 3.5 ms and 4 ms for the green curve.

2.2. Conduction delays in the connections

In order to study the effect of an explicit axonal conduction delay in the connections, we perform numerical simulations with two reciprocally coupled HH neurons. In Figure 2.2 we plot the synchronization index (see Section 1.4.2) as a function of the delay for two excitatory coupled neurons (red) and for two inhibitory coupled pair (green), for a fixed value of the coupling strength. As before, an index value of zero means in-phase synchronization, whereas a value of one represents an anti-phase state.

In the excitatory case, for low delay values the synchronization index is zero, thus the neurons are synchronized in-phase. This behavior can be understood from the PRC. The neuron that fires earlier in an oscillatory cycle advances the spike time of the other neuron (later firing), which in turns delays the spike of the earlier firing neuron [2]. Both neurons adjust their timing and they finally spike in-phase. This is observed for type II PRC neurons coupled by fast excitatory synapses [32] (see Figure 2.3 as an example).

As the delay is increased the anti-phase solution emerges. For delays close to multiples of the natural period of firing ($T_0 = 14.65$ ms), the in-phase solution appears for excitatory synapses. Changes in the delay time reveal a resonant effect in the synchronization. On the contrary, for inhibitory synapses the opposite behavior is observed, when the delay is small the neurons are synchronized in anti-phase and a transition to an in-phase solution is observed as the delay is increased. If the delays are close to multiples of the

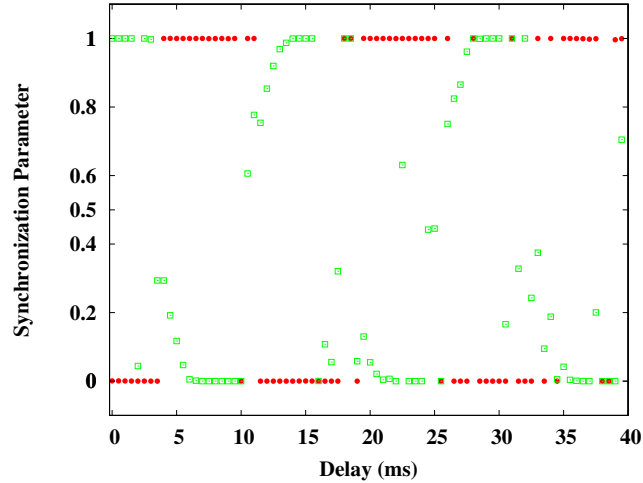


Figure 2.2: Synchronization index of two fast coupled HH neurons as a function of the delay in the connections, for fast excitatory (red dots) and fast inhibitory (green dots) synapses. In this case the rise time is 0.1 ms and the decay time is 3 ms. A resonant effect is observed, switching between the in-phase to anti-phase solutions. In both cases the coupling is weak, it is set to $g_{max} = 0.15 \text{ mS/cm}^2$.

natural period the anti-phase solution emerges.

In the last section we described how the PRC of a HH regular spiking neuron changes with the rise time of the synapse. Now we will see how the synchronization properties of a pair of coupled neurons are modified by the PRC change. A pair of coupled neurons loses its ability to synchronize in-phase subject to excitatory synapses without delay, see Figure 2.4. If the delay is non zero and close to multiples of the natural period the neurons are synchronized out of phase. Only for smaller values of the delay, relative to the natural period, the neurons synchronize in-phase. We observe a resonant effect but for delays shifted with respect to the natural period (Figure 2.2). In the case that the coupling is inhibitory the opposite behavior is observed.

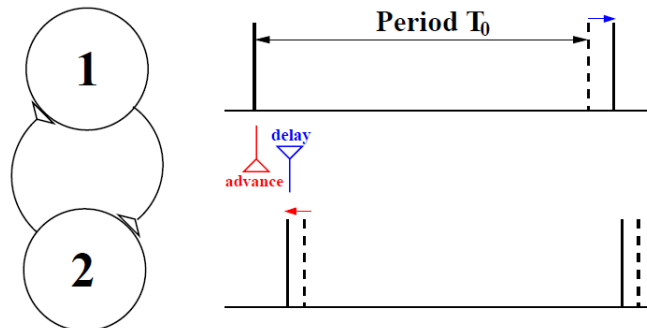


Figure 2.3: Schematic diagram of two excitatory coupled neurons: fast mutual excitation synchronizes in-phase neurons with type II PRC (as the HH model). The natural period of oscillations in the absence of perturbation is T_0 , the dashed line represents the spike time of isolated neurons and the solid line the perturbed spikes. In the diagram the neuron number 1 fires earlier, the effect of this spike in neuron number 2 advances the next spike. Whereas, the effect of the spike of neuron 2 delays the next spike of neuron 1, reducing phase differences in the next cycles. Figure adapted from [2].

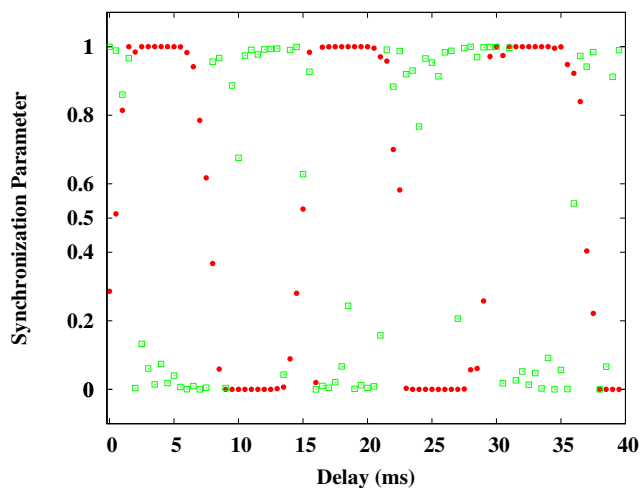


Figure 2.4: Synchronization index of two slow coupled HH neurons as a function of the delay, for slow excitatory (red dots) and slow inhibitory (green dots) synapses. In this case the time rise is 6 ms and the time decay is 3 ms.

Chapter 3

Neural Networks

In the previous chapter we have studied the effect of the delay in the connections in a pair of coupled neurons, as well as the effects that other factors have in the synchronization (e.g., the type and time of the synapses). In this section, we investigate how the topology of a network affects the synchronization properties. With this purpose, we implement an ensemble of neurons reciprocally connected placed in different network topologies (regular, small world, etc.). We explore the stability of the solutions and study how do they change with the delay, as we did before, for a pair of coupled neurons (see Chapter 2).

3.1. Effects of the topology

3.1.1. Homogeneous delay

We begin by considering an ensemble of identical neurons, whose dynamical behavior is described by the Hodgkin and Huxley model [11]. The network is composed by $N=10^3$ units, connected with reciprocal delayed chemical couplings, modeled as two exponential functions (see Section 1.3). In the network, each neuron is connected on average with four neighbors. We start considering fast excitatory synapses, with rise and decay times 0.1 ms and 3 ms, respectively. We concentrate on the response of the system when all the units are in a regular spiking regime, subject to an external bias density current of $I=10 \mu\text{A}/\text{cm}^2$.

We study the influence of different topologies on the local and global synchronization properties of the network (see Section 1.4.2). We analyzed five different types of topologies: regular, small-world, random, scale-free and all-to-all (see Section 1.5).

Figure 3.1 shows the contour plot of S^{loc} and S^{glob} when the coupling between the neurons and the delay in the connections vary for a regular, small world, random, scale free and an all-to-all network. Changes in the delay time reveal a resonant effect in the synchronization as in the case of two coupled

spiking neurons (Chapter 2). In-phase solutions (white regions in Figure 3.1) appear for delays close to (or multiple of) the natural period of the neurons corresponding, in this case, to $T_0 = 14.65$ ms. These in-phase regions slightly shift when the coupling strength increases, probably caused by a small reduction of the natural period due to the stronger interaction. At a local scale, the regular, small-world, random and scale free networks exhibit also anti-phase synchronization (blue regions in top panel Figure 3.1) where the neurons fire in two clusters with a difference of phase π between them. This dynamical regime is not observed in the fully connected network. Between the in-phase and anti-phase regimes we also find regions where the neurons fire in an out-of-phase regime (green areas in Figure 3.1).

Interestingly, while synchronized firing activity between one neuron and its neighbors (local synchronization) is found in all networks that were considered, a high randomness in the connections is required for a coherent global synchronized activity. From Figure 3.1 it can be observed that the random network exhibits regions of global synchronization that are not present in the regular or small world networks. This global synchronized activity is also found in the scale-free and all to all network. These results might be relevant for the brain, where certain diseases, like Alzheimer or Schizophrenia [3], are associated with synchronization aspects (decreasing or increasing synchronized activity) and also with a change in the functional topology.

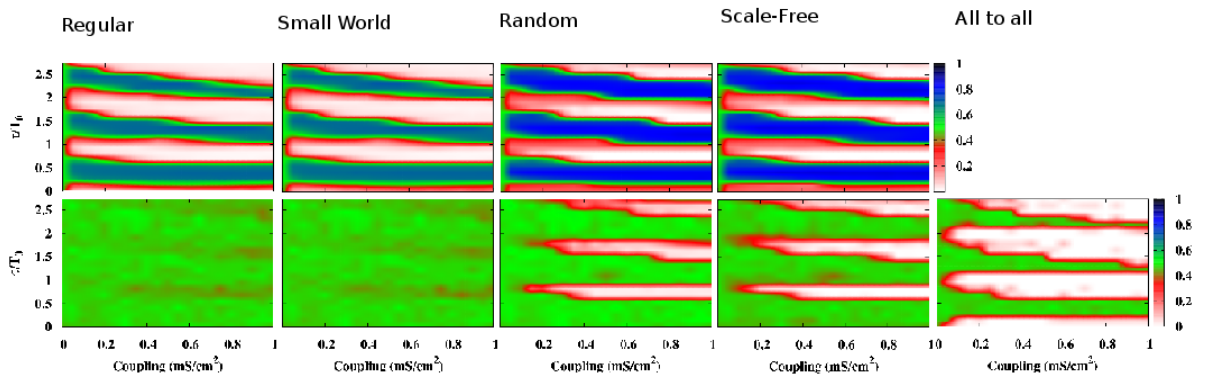


Figure 3.1: Local and global synchronization indexes for the different network topologies as a function of both the coupling strength and the delay in the connections. An index value of zero represents an in-phase state, whereas a value of one represent an anti-phase state.

To illustrate the activity of the network, we show in Figure 3.2 raster plots of 100 neurons, for a regular, random and scale-free topologies. In the right y-axis we plot the value of the synchronization index. From top to bottom rows the value of the delay is set to 12, 14 and 16 ms respectively. It can be seen how the local synchronization is lost for higher delay values. From left to right we can observe how a global synchronized state emerges when we vary the topology of the network, from a regular to random and scale free.

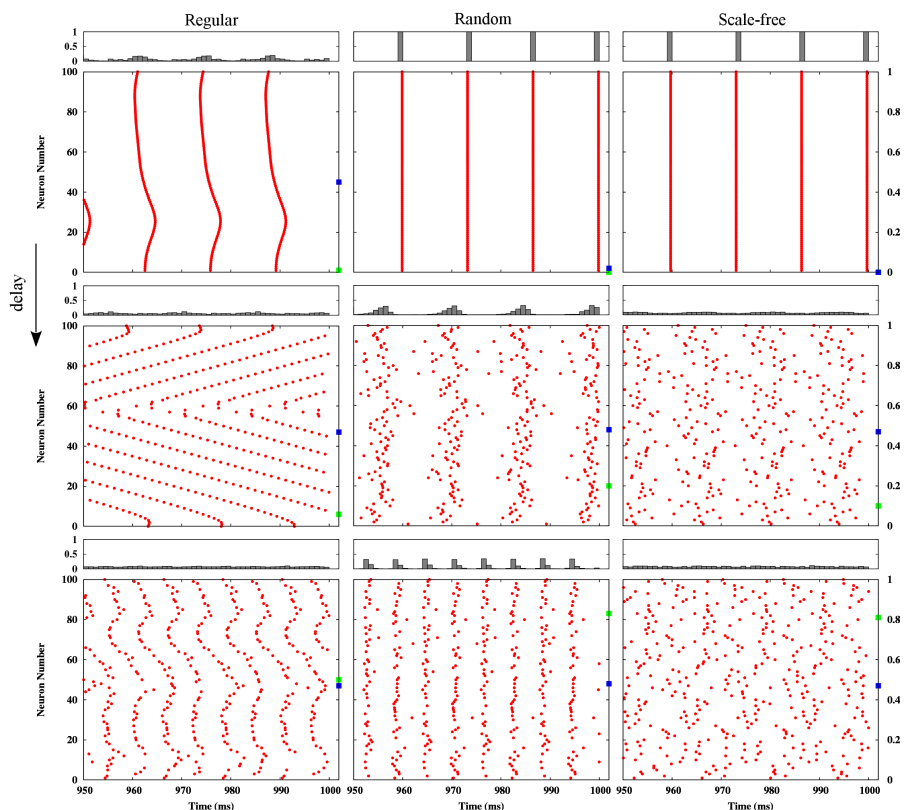


Figure 3.2: Raster plots of spikes for 100 neurons for different network topologies. The coupling strength is fixed to 0.8 mS/cm^2 and delays are: 12-14-16 ms (from top to bottom). On the right y-axis it is plotted the value of the local (green) and global (blue) synchronization index.

As we mentioned before, for a motif of two neurons reciprocally coupled (Chapter 2), the delay can change the stability of the solutions. If the neurons are connected via excitatory synapses they synchronize in-phase without delay and for delays multiples of the natural period, and they synchronize in anti-phase in other cases. Interestingly, if the neurons are immersed in a network, local the dynamics is the same, as it is reflected in the local synchronization index. In our network each neuron is connected on average to four neighbors. However, it could happen that the local dynamics differs if the neurons were connected with more than four neurons.

A pair of coupled neurons connected by inhibitory synapses synchronize in anti-phase without delay or with delays multiples of the natural period. To compare this situation with a network, we performed numerical simulations in a network of randomly connected neurons coupled via inhibitory synapses. In Figure 3.3 we plot the local and global synchronization indexes for this case. As in the case of two coupled neurons, for delays multiples of the natural period the neurons synchronize in anti-phase. In the same way, the delay

changes the stability of the solutions, as it is reflected in the local synchronization index.

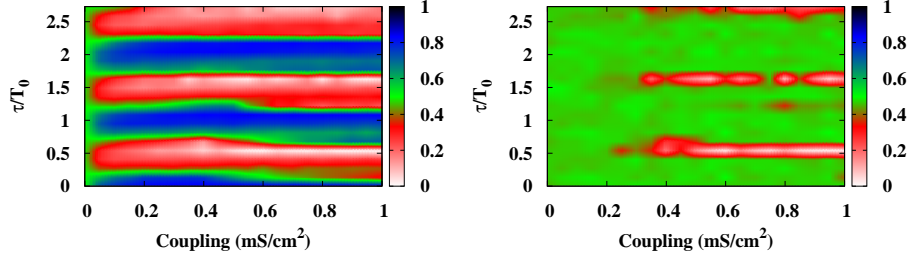


Figure 3.3: Local and global synchronization indexes for a random network as function of both the coupling strength and the delay in the connections. In this case the neurons are connected via fast inhibitory synapses

3.1.2. Heterogeneous delays

To gain insight into the effects of the delay in the synchronization properties we consider heterogeneous delays in the connections. We explore different possible distributions chosen from a general gamma distribution function, with probability density function given by:

$$f(\tau) = \tau^{k-1} \frac{\exp\left(\frac{-\tau}{\theta}\right)}{\theta^k \Gamma(k)}, \quad (3.1)$$

where k and θ are shape and scale parameters of the γ distribution. The mean delay of the distribution is given by $\langle \tau \rangle = k\theta$ and the variance by $\sigma^2 = k\theta^2$. We implemented two configurations: one in which the variance of the distribution is maintained fixed and another in which the variance is varied proportional to the mean value of the delay. In both configurations the mean value of the delay is varied between 0.2 to 40 ms (as in the homogeneous case).

As it happens with the homogeneous configuration, heterogeneous delays also develop a resonant effect in the synchronization indexes (even in the all-to-all topology), as it is shown in the Figure 3.4-3.5. This effect is clearly reflected in the shape of the local synchronization index (top panel Figure 3.4-3.5). To reach a global synchronized state, we find that a high randomness in the connections is required (middle panel Figure 3.4-3.5), although this effect is lost when the variance of the delay distribution is $\sim 2 \text{ ms}^2$ or larger. Whereas, the scale free topology is more robust and maintain certain globally synchronized regions even for large variances in the distribution of delays (bottom panels Figure 3.4-3.5).

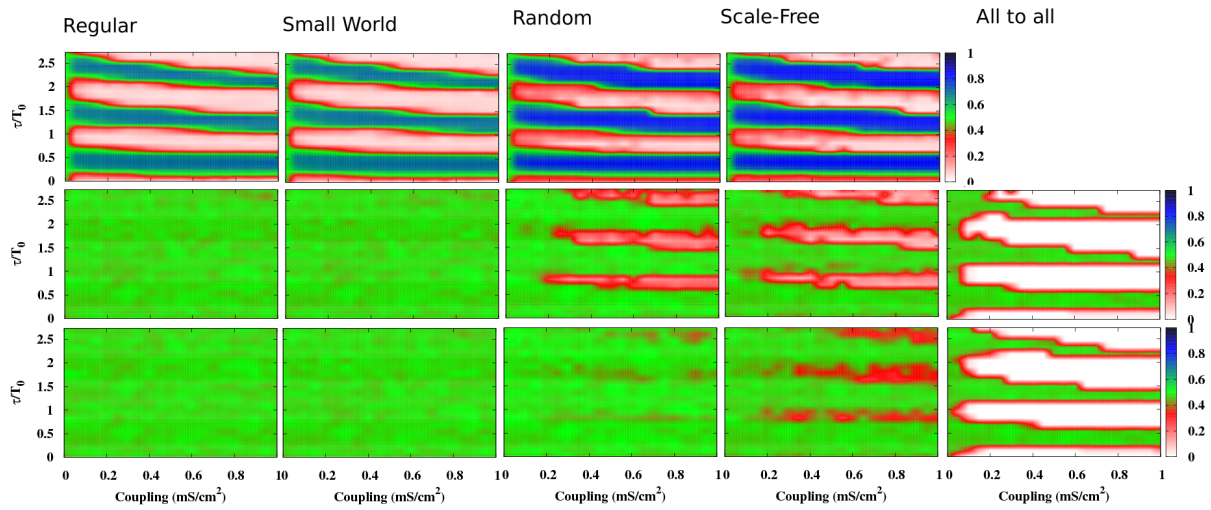


Figure 3.4: Local and global synchronization indexes for different network topologies as a function of both the coupling strength and the mean delay in the connections. Delays were generated according to a gamma distribution. The mean value is varied between 0.2 to 40 ms, and the variance is kept constant at 0.5 ms^2 in the middle panel and 2 ms^2 in the bottom one.

To characterize the different states of the system we display raster plots of a fraction of the neurons, for regular, random and scale free topologies (Figure 3.6). From top to bottom rows the value of the delay is set to 12, 14 and 16 ms respectively. Local synchronization is lost for large delay values. From left to right it can be observed how a global synchronized state emerges when we vary the topology of the network (from regular to random and scale-free). The values of the synchronization indexes are almost the same, as compared to the case of homogeneous delays.

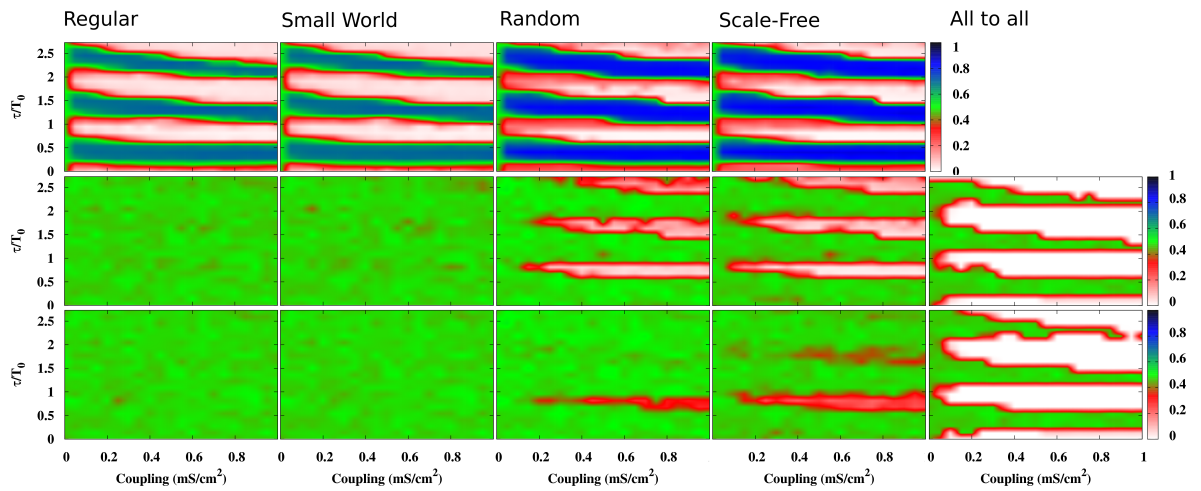


Figure 3.5: Local and global synchronization indexes for different network topologies as a function of both the coupling strength and the mean delay in the connections. Delays were generated according to a gamma distribution. The mean value is varied between 0.2 to 40 ms, and the variance is kept proportional to the delay, at 1 % of the mean delay in the middle panel and 10 % of the mean delay in the bottom one.

The main difference with respect to the homogeneous case in the random network resides at the mean firing rate of the neurons. In the heterogeneous case, the mean firing rate is almost flat for mean delays 14 and 16 ms while for the same values in the homogeneous distribution there is still a level of synchronization reflected in the mean firing rate.

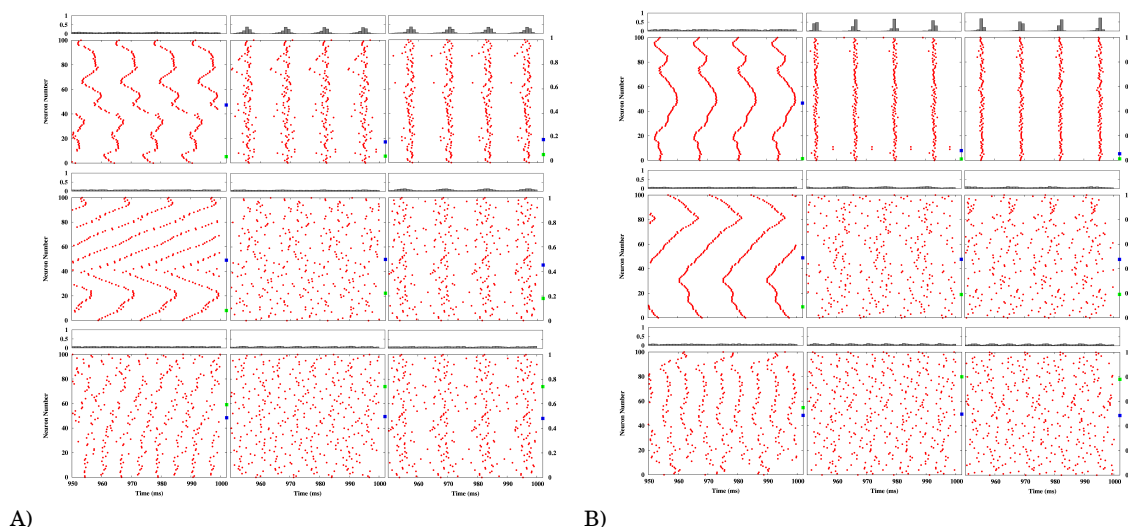


Figure 3.6: Raster plots of a fraction of the neurons for a regular, random and scale free topologies (from left to right in each panel A and B). The coupling strength is 0.8 mS/cm^2 and delays are 12-14-16 ms from top to bottom. On the right y-axis it is plotted the value of the local (green) and global (blue) synchronization indexes. In panel A the variance is kept constant at 0.5 ms^2 while in panel B the variance is assumed to be proportional to 1% of the mean delay.

3.1.3. Heterogeneous currents

The assumption considered up to now, that all the neurons in the network are in a regular spiking regimen is an ideal situation. For this reason, and with the aim of exploring a more realistic situation, we allow the natural frequencies of the neurons to be different to each other. In the Hodgkin-Huxley model, the pulsating frequency of the neurons depends on the injected current I_0 . Thus, we modeled the dispersion of frequencies by assuming that each neuron receives an external density current that follows a Gaussian distribution with mean value $I_0 = 9 \mu\text{A/cm}^2$ and dispersion $\sigma_{I_0} = 2.5 \mu\text{A/cm}^2$, allowing some neurons to operate in the sub-threshold state. It is known that a single HH-type neuron enters into a periodic regime if the external current is greater than $\sim 6 \mu\text{A/cm}^2$ (if the initial current is zero) [14]. Consequently, in our simulation $\sim 10 \%$ of the neurons are in a steady state before the coupling is turned on and also for low coupling strength.

The effect of the distribution of natural frequencies requires an increase of the coupling strength needed to achieve a global synchronous state, as it can be seen in Figure 3.7. The global synchronized regions are reduced for almost all networks that we have considered. Nevertheless, in the fully connected case, the synchronized area quasi merges in a single region at high coupling values, almost losing the resonant character of the delay. As in the homogeneous frequency case, three different states of in-phase, out-of phase and anti-phase appear for S^{loc} (see Figure 3.7) although these regions are shifted

with respect to the homogeneous case.

Moreover, global in-phase synchronization is more difficult to achieve and only the random and the scale-free networks exhibit this state at high coupling intensities but only for some particular values of the delay time. In all the cases the predominant state is the one in which the neurons spike without a well defined phase relationship corresponding to the out-of-phase state indicated by green areas in Figure 3.7.

Another important observation that can be pointed out from the present analysis concerns the annihilation of repetitive firing observed in some neurons in the networks. As we mentioned before, for low coupling $\sim 10\%$ of the neurons are in an excitable state (they do not fire when isolated), as it is shown in the Figure 3.7. Enhancing the coupling strength the number of non-firing neurons increases, reaching a maximum value for couplings $\sim 0.15 \text{ mS/cm}^2$. As it is expected, increasing further the coupling all the neurons reach the regular firing regime.

Experimental and theoretical investigations have been carried out to understand the mechanisms by which repetitive firing are suppressed by short pulses [35, 36]. It was computationally verified that a stable and an unstable periodic solution coexist with a stable singular point for a particular interval of injected currents in the Hodgkin and Huxley model [36]. As far as we know, the suppression of repetitive firings was not reported before in a network of Hodgkin and Huxley neurons.

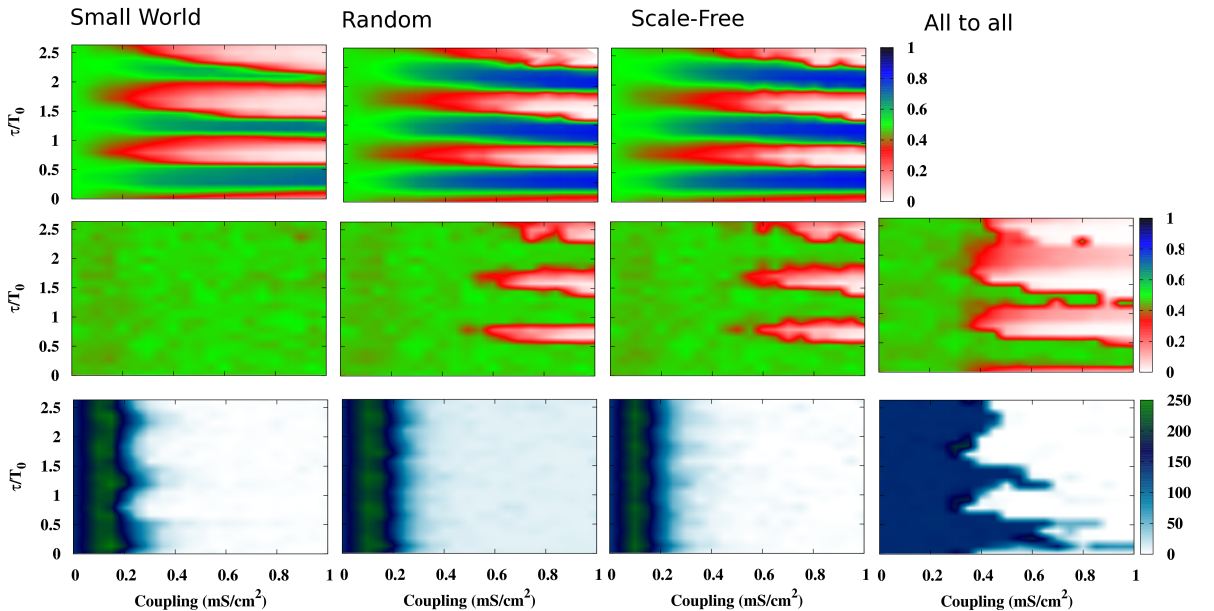


Figure 3.7: Contour plots of local and global synchronization indexes (top-middle panels) in the coupling delay-phase space for a heterogeneous ensemble of neurons, and for different topologies. Density plots of the number of non-spiking neurons (bottom panel).

Chapter 4

Conclusions

To summarize, we have performed extensive numerical simulations of coupled Hodgkin-Huxley neurons to uncover the collective behavior in different networks.

First, we have studied synchronization properties of a pair of coupled neurons, and we have explored the effects of the synapse timings and the types of synapses on the PRC of an isolated neuron. We correlated the synchronization phenomena with the shape of the PRC, and then we compared these results with those of a network of neurons reciprocally connected.

Second, we observed that only certain network topologies allow for a coordinated firing at both local and long-range scale simultaneously. At a local level, we found that all the considered topologies exhibit three different operating regimes: in-phase, out-of-phase and anti-phase. Besides the network architecture, axonal conduction delays are also observed to play an important role in the generation of coherent dynamic. Such communication latencies not only set the phase difference between the oscillatory activity of remote neurons but also determine whether the interconnected cells can set in a coherent firing or not.

Third, the effect of heterogeneous delay in the dynamics of coupled neurons was also explored. On the one hand, global synchronization in a random network is lost when the variance of the delay distribution is large ($\sigma^2 \sim 2 \text{ ms}^2$). On the other hand, the scale free topology is more robust and maintain globally synchronized regions even for large variances in the distribution of delays.

Finally, we have also investigated the effects of inhomogeneities in natural firing frequencies on the synchronization properties. The presence of inhomogeneities in the frequency difficults the occurrence of coordinated firing states. When neurons are not identical, but possess a certain distribution of the natural frequencies of firing, the region of phase synchronization decreases emphasizing the importance of having small diversity in the system for a coherent response to occur.

Besides the mechanisms studied here, other aspects could be consider as

well. Inhibitory neurons and mixed networks of type I and II PRC might play a significant role and will be consider in detail in future studies.

Bibliography

- [1] A. S. Pikovsky, M. G. Rosenblum, and J. Kurths, *Synchronization: A universal concept in nonlinear sciences*. Cambridge University Press, 2001.
- [2] X. J. Wang, “Neurophysiological and computational principles of cortical rhythms in cognition,” *Physiological Reviews*, vol. 90, July 2010.
- [3] P. J. Uhlhaas and W. Singer, “Abnormal neural oscillations and synchrony in schizophrenia,” *Nature Reviews Neuroscience*, vol. 11, pp. 100–113, 2010.
- [4] E. R. Kandel, “Nerve cells and behavior,” in *Principles of Neural Science* (E.R.Kandel and J.H.Schwartz, eds.), ch. 2, Elsevier, 1985.
- [5] C. Giaume, A. Koulakoff, L. Rouz, D. Holcman, and N. Rouach, “Astroglial networks: a step further in neuroglial and gliovascular interactions,” *Nature Reviews Neuroscience*, vol. 11, pp. 87–99, 2010.
- [6] P. Dayan and L.F.Abbott, *Theoretical Neuroscience, Computational and Mathematical Modeling of Neural Systems*. The MIT Press, 2001.
- [7] E. M. Izhikevich, *Dynamical Systems in Neuroscience: The Geometry of Excitability and Bursting*. The MIT Press, 2007.
- [8] J. Keener and J. Sneyd, *Mathematical Physiology*. Springer Verlag, 1998.
- [9] J. Rinzel, “Intercellular communication,” in *Computational Cell Biology* (C. P. Fall, E. S. Marland, J. M. Wagner, and J. J. Tyson, eds.), Springer-Verlag, 2002.
- [10] K. S. Cole and H. J. Curtis, “Electrical impedance of squid giant axon during activity,” *J.Gen.Physiol.*, vol. 22, pp. 649–670, 1939.
- [11] A. L. Hodgkin and A. Huxley, “A quantitative description of membrane current and its application to conduction and excitation in nerve,” *Journal of Physiology*, vol. 117, pp. 500–544, 1952.
- [12] J. Koester, “Voltage-gated channels and the generation of action potentials,” in *Principles of Neural Science* (E.R.Kandel and J.H.Schwartz, eds.), ch. 9, Elsevier, 1985.

- [13] E.R.Kandel and S. A. Siegelbaum, "Overview of synaptic transmission," in *Principles of Neural Science* (E.R.Kandel and J.H.Schwartz, eds.), ch. 10, Elsevier, 1985.
- [14] W. Gerstner and W.M.Kistler, *Spiking Neuron Models, Single Neurons, Populations, Plasticity*. Cambridge University Press, 2002.
- [15] R. M. Smeal, G. B. Ermentrout, and J. A. White, "Phase-response curves and synchronized neural networks," *Phil. Trans. R. Soc. B*, vol. 365, pp. 2407–2422, 2010.
- [16] S.H.Strogatz, *Nonlinear Dynamics and Chaos: with applications to physics, biology, chemistry and engineering*. Addison-Wesley, 1994.
- [17] R. F. Galán, "The phase oscillator approximation in neuroscience: An analytical framework to study coherent activity in neural networks," in *Coordinated Activity in the Brain Measurements and Relevance to Brain Function and Behavior* (J. L. P. Velazquez and R. Wennberg, eds.), pp. 65–89, Springer Series in Computational Neuroscience, 2009.
- [18] A. T. Winfree, *The Geometry of Biological Time*. Springer-Verlag, 1980.
- [19] L. Glass and M. C. Mackey, *From clocks to chaos : The rhythms of Life*. Princeton University Press, 1988.
- [20] B. Ermentrout and N. Kopell, "Multiple pulse interactions and averaging in coupled neural oscillators," *J. Math. Biol.*, vol. 29, pp. 195–217, 1991.
- [21] B. Ermentrout, *Simulating, Analyzing, and Animating Dynamical Systems: A Guide to Xppaut for Researchers and Students*. SIAM, 2002.
- [22] R. F. Galán, B. Ermentrout, and N. N. Urban, "Efficient estimation of phase-resetting curves in real neurons and its significance for neural-network modeling," *Phys. Rev. Lett*, vol. 94, pp. 158101–4, 2005.
- [23] T. Tateno and H. Robinson, "Phase resetting curves and oscillatory stability in interneurons of rat somatosensory cortex," *Biophysical Journal*, vol. 92, pp. 683–695, 2007.
- [24] R. Albert and A. Barabasi, "Finding and evaluating community structure in networks," *Rev. Mod. Phys.*, vol. 74, pp. 47–97, 2002.
- [25] S. Boccaletti, V. Latora, Y. Moreno, M. Chavez, and D. U. Hwang, "Complex networks: Structure and dynamics," *Physics Reports*, vol. 424, pp. 175–308, 2006.
- [26] S.N.Dorogovtsev and J.F.F.Mendes, *Evolution of Networks, From Biological Nets to the Internet and WWW*. Oxford University Press, 2003.

- [27] A. Arenas, A. Diaz-Guilera, J. Kurths, Y. Moreno, and C. Zhou, "Synchronization in complex networks," *Physics Reports*, vol. 469, pp. 93–153, 2008.
- [28] P. Erdos and A. Rényi, "On the evolution of random graphs," *Publ. Math. Inst. Hung. Acad. Sci.*, vol. 5, p. 1761, 1960.
- [29] E. Bullmore and O. Sporns, "Complex brain networks: graph theoretical analysis of structural and functional systems," *Nature Reviews Neuroscience*, vol. 10, pp. 186–198, March 2009.
- [30] D.J.Watts and S.H.Strogatz, "Collective dynamics of small-world networks," *Nature*, vol. 393, pp. 440–442, 1998.
- [31] A.L.Barabasi and R.Albert, "Emergence of scaling in random networks," *Science*, vol. 286, no. 5439, pp. 509–512, 1999.
- [32] D. Hansel, G. Mato, and C. Meunier, "Synchrony in excitatory networks," *Neural Computation*, vol. 7, pp. 307–337, 1995.
- [33] C. V. Vreeswijk, L.F.Abbott, and G.B.Ermentrout, "When inhibition not excitation synchronizes neural firing," *Journal of Computational Neuroscience*, vol. 1, pp. 313–321, 1994.
- [34] G.B.Ermentrout, "Type i membranes, phase resetting curves, and synchrony," *Neural Computation*, vol. 8, no. 5, pp. 979–1001, 1996.
- [35] R. Guttman, S. Lewis, and J. Rinzel, "Control of repetitive firing in squid axon membrane as a model for a neuron oscillator," *J. Physiol.*, vol. 305, pp. 377–395, 1980.
- [36] J. Rinzel and R.N.Miller, "Numerical calculation of stable and unstable periodic solutions to the hodgkin-huxley equations," *Mathematical Biosciences*, vol. 49, pp. 27–59, 1980.

Curriculum Vitae

Guadalupe C. García

Isaac Peral, 2 3B
E-07004 Palma de Mallorca
guadagar@gmail.com
+34 635 15 1000

Personal data

Birth date and place: 27/09/1980, Buenos Aires, Argentina

Nationality: Argentina

Education background

- 2009-2010: Master in Physics at the Universidad de las Islas Baleares
Palma de Mallorca, España.
Thesis title: *“Effects of the topology and delayed connections in the synchronization properties of a neuronal network”*.
Thesis directors: Claudio Mirasso and Victor Eguíluz.
- 2000-2007: Physics studies at Universidad de Buenos Aires, Argentina
Obtained degree: Licenciatura en Ciencias Físicas.
Thesis title: *“A Biophysical Model of the Peripheral Auditory System”*.
Thesis director: Manuel C. Eguía.
Grade Point Average: 9.15 (1 to 10 scale).

Other skills

Programming: Fortran, Matlab
Languages: Spanish (native)
English (fluent)
German (A1.2)

Publications

2006: Granada A., Gabitto M., García G.C., Alliende J., Méndez

- J., Trevisan M.A. and Mindlin G.B, "*The generation of respiratory rhythms in birds*", *Physica A*, 371 pp 84-87, 2006.
- 2008: Eguía M.C., García G.C. and Romano S.A., "*A Biophysical Model for Modulation Frequency Encoding in the Cochlear Nucleus*", *Journal of Physiology-Paris*, 104 pp 118-127, 2010.
- 2010: T. Perez, G.C. García, V.M. Eguíluz, R. Vicente, G. Pipa and C. Mirasso, "*Effects of the topology and delayed interactions in the coordination of neuronal firing*", Submitted.

Participation in Conferences:

- 2005: "*Measure of air sac pressure in singings birds*", 90th meeting of the Asociación Física Argentina (AFA), La Plata, Argentina. Poster contribution.
- 2006: "*The generation of respiratory rhythms in birds*", 8th Winter School J. J. Giambiagi, B Physics and Biology Reloaded, Physics Department, FCEyN, University of Buenos Aires, Argentina, from July 31 to August 4. Poster contribution.
- 2007: "*Envelope encoding in neurons of the ventral cochlear nucleus*", 7th International Neural Coding Workshop, Montevideo, Uruguay, from November 5 to 12.
- 2008: "*A biophysical model of the peripheral auditory system*", X Taller Argentino de Neurociencias, Huerta Grande, Córdoba, Argentina, from April 9 to 13. Poster contribution.
- 2008: "*Encoding of amplitude modulated sounds in the auditory nerve*", Neurolatam I Congress IBRO/LARC of Neurosciences for Latin American, Caribbean and Iberian Peninsula, Buzios, Brazil, from September 1 to 4. Poster contribution.
- 2009: "*Effects of topology and delayed connections in the synchronization properties of a neural network*", 8th International Neural Coding Workshop, Tainan, Taiwan, from May 8 to 13. Poster contribution.
- 2009: "*Effects of topology and delayed connections in the synchronization properties of a neural network*", XIII Congreso de la Sociedad Española de Neurociencia, Tarragona, Spain, from September 16 to 19. Poster contribution.

2010: 16th Annual Meeting of the Organization for Human Brain Mapping, Barcelona, Spain, from June 6 to 10.

Informal Talks

2008: “A Biophysical Model for Modulation Frequency Encoding in the Cochlear Nucleus”, Frankfurt Institute for Advanced Studies, Frankfurt, Germany, August 26.

2009: “A biophysical model of the peripheral auditory system”, Institute for Cross-Disciplinary Physics and Complex Systems, Palma de Mallorca, Spain, July 07.

Workshops and Summer Schools

2008: FENS summer school: “Theoretical Neuroscience and Complex Systems”, hosted by the Frankfurt Institute for Advanced Studies, Frankfurt, Germany from August 2 to 24.

2009: “Effects of the topology and delayed connections in the synchronization properties of a neural network”, Trends in Complex Systems: Synchronization and Multi-scale Complex Dynamics in the brain workshop, organized by the Max Planck Institut für komplexer Systeme and the Institute for Cross-Disciplinary Physics and Complex Systems, Dresden, Germany, from November 2 to 6. Poster contribution.

2010: FENS-IBRO summer school: “Advanced Course in Computational Neuroscience”, hosted by the Bernstein Center for Computational Neuroscience, Freiburg, Germany from August 2 to 27.

Grants

Sarmiento Grant, financial aid grant sponsored by the University of Buenos Aires, March 2004-December 2007.

PhD scholarship awarded by Consejo Nacional de Investigaciones Científicas y Técnicas, April 2008 to November 2008.

Collaboration Scholarship associated to different European projects (Picasso-GABA) for research at the Institute for Cross-Disciplinary Physics and Complex Systems (UIB-CSIC), from November 2008 to November 2009.

Master scholarship awarded by the Universitat de las Islas Baleares (Telefónica Iberoamérica), December 2009 to November 2010.

Teaching Experience

Teaching Assistant at the University of Buenos Aires, CBC, Mathematics Department, from March to July 2004 (two positions), from March 2005-November 2008 (one position) (Course to be admitted at the University).

Teaching Assistant, Physics Department, FCEyN, University of Buenos Aires. Courses taught: Laboratory 3, Electricity and Magnetism. From August 2004 to March 2005. Physics for biologists 1. From August 2005 to March 2006.

Teaching Assistant at the University of Buenos Aires, CBC, Physics Department, from March 2005 to April 2008 (two positions). (Course to be admitted at the University). Courses taught: Physics and Biophysics.

September 16, 2010